

Ambient Backscatter Communication Systems: Detection and Performance Analysis

Gongpu Wang, Feifei Gao, Rongfei Fan, and Chintha Tellambura, *Fellow, IEEE*

Abstract—Ambient backscatter technology that utilizes the ambient radio frequency (RF) signals to enable the communications of battery-free devices has attracted much attention recently. In this paper, we study the problem of signal detection for an ambient backscatter communication system that adopts the differential encoding to eliminate the necessity of channel estimation. Specifically, we formulate a new transmission model, design the data detection algorithm, and derive two closed-form detection thresholds. One threshold is used to approximately achieve the minimum sum bit error rate (BER) while the other yields balanced error probabilities for “0” bit and “1” bits. The corresponding BER expressions are derived to fully characterize the detection performance. In addition, the lower and the upper bounds of BER at high signal noise ratio (SNR) regions are also examined to simplify performance analysis. Simulation results are then provided to corroborate the theoretical studies.

Index Terms—Ambient backscatter, RF-powered device, maximum likelihood (ML) detection, BER, battery-free tag.

I. INTRODUCTION

Radio Frequency Identification (RFID) systems have attracted increasing attentions from both academic circles and industrial communities over the past two decades [1]. According to IDTechEx [2], the total RFID market, including tags, readers and software/services for RFID components, was worth \$8.89 billion in 2014, up from \$7.77 billion in 2013 and \$6.96 billion in 2012, and is forecast to rise to \$27.31 billion in 2024.

A typical RFID system mainly consists of a reader (also known as an interrogator) and a tag (also known as transponder). Depending on the tag’s power supply, RFID systems can be active, passive or semi-passive [3]. For passive RFID, the reader first generates an electromagnetic wave, and the tag receives and backscatters the wave with modulated information bits to the reader.

Clearly, passive RFID systems essentially relies on radio backscatter, a mode of wireless communication by means of

Manuscript received January 27, 2016; revised June 2, 2016 and August 1, 2016; accepted August 11, 2016. This study is supported by the National Natural Science Foundation of China (No. 61571037) and by the Fundamental Research Funds for the Central Universities (No. 2014JBZ003).

Part of this work has been presented at the IEEE Global Communications Conference (IEEE Globecom), San Diego, CA, USA, 2015 [24].

G. Wang is with Beijing Key Lab of Transportation Data Analysis and Mining, School of Computer and Information Technology, Beijing Jiaotong University, Beijing, China, 100044. Email: gpwang@bjtu.edu.cn.

F. Gao (corresponding author) is with Department of Automation, Tsinghua University, State Key Lab of Intelligent Technologies and Systems, Tsinghua National Laboratory for Information Science and Technology (TNList) Beijing, 100084, P.R. China. Email: feifeigao@ieee.org.

R. Fan is with School of Information and Electronics, Beijing Institute of Technology, Beijing, China, 100081. Email: fanrongfei@bit.edu.cn.

C. Tellambura is with the Department of Electrical and Computer Engineering, University of Alberta, Edmonton, AB, Canada, T6G 2V4. Email: chintha@ece.ualberta.ca.

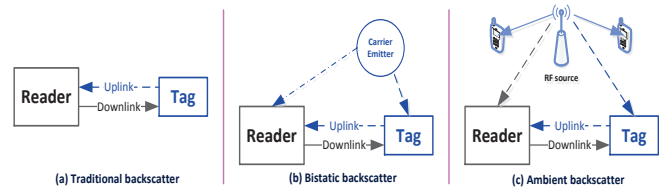


Fig. 1. Three types of backscatter.

reflection rather than radiation. The origin of radio backscatter dates back to World War II when the radio signal transmitted by some radar and backscattered from an on-coming airplane was used to identify it as “friend or foe” [3]. Backscatter communication was first described by Harry Stockman in 1948 [4]. Since then, it has been continuously studied and RFID products have been developed for identification/supply chain applications. From 1990 to 2000, a famous and successful application of RFID systems was Electronic Toll Collection (ETC) that can enable vehicles on the high speedways to pay the toll fee without stopping. After the 1990s, the rapid progress in integrated circuits decreased the cost of tags, which enabled the wide-spread usage of RFID products and also aroused great interests on further investigation of the backscatter technology. In past ten years, extensive studies about radio backscatter have been performed on coding methods [5], channel fading and modelling [8], link budgets [6], [7] and multi-antenna techniques [9], etc. Other applications include sensor networks and Internet of things (IoT) due to its capability in reducing energy and monetary cost [1], [13], [10]. In addition, the problems of RFID privacy and backscatter physical-layer security have received research interest [11], [12].

As shown in Fig. 1(a), the traditional backscatter¹ requires that the reader generate a continuous carrier wave that will be received and remodulated by the tag [5]. This process incurs a round-trip path loss, which will impose a limit on the communication distance between the reader and the tag [6], [8], [9], [27].

To further increase the field coverage and communication range or avoid the round-trip path loss, bistatic scatter [13] and ambient backscatter [14], [15] have been proposed. Bistatic scatter was suggested in [13] to enlarge the communication distance through dislocating the carrier emitter from the reader (Fig. 1(b)) and setting the emitter close to the tag. On the other side, ambient backscatter utilizes ambient radio frequency

¹For brevity, we refer the radio scatter between one reader and one tag as traditional backscatter, so as to distinguish it from bistatic scatter and ambient backscatter introduced later.

(RF) signals, such as television (TV) radio, cellular signals, and Wireless Fidelity (Wi-Fi), to enable battery-free tag to communicate with the reader [14], [15]. As depicted in Fig. 1(c), the tag is illuminated by ambient wireless signals instead of fixed-frequency sine/cosine waves.

The key idea of the ambient backscatter is as follows [14]: (i) The battery-free devices such as a tag or a sensor can transmit “0” or “1” bit through switching the antenna between reflecting and non-reflecting states, i.e., a change of the tag antenna impedance states; (ii) the battery-free device can backscatter its own information at a much lower data rate than the ambient signals so that the receiver can separate the two signals through averaging. Based on this idea, the authors [14] devised a prototype where two battery-free devices communicate via ambient backscatter and demonstrate its practical bit error rate (BER) versus distance. In 2014, Wi-Fi backscatter was designed to connect the battery-free devices with off-the-shelf Wi-Fi devices [15]. In 2015, full-duplex technology was introduced with WiFi access point (AP) to cooperate with backscatter to enlarge data throughput [16]. It was shown recently that Bluetooth transmissions can be leveraged to create Wi-Fi and ZigBee-compatible signals utilizing backscatter communication [17].

Such a new ambient backscatter technology can enable battery-free devices to communicate mutually or connect to the Internet. It can also enable ubiquitous communication among pervasive devices, liberate sensor nodes from maintenance-heavy batteries [14], and may even bring a new generation of RFID [19], [20]. Nevertheless, a fully developed theory on signal processing and performance analysis for ambient backscatter communication systems is fundamentally different from that of traditional communication systems and hence this field completely warrants further research [24].

Despite so many promising aspects, as a new-born thing, ambient backscatter also raises up a series of open problems. The first is wireless power extraction and utilization at the tag or the sensor. Secondly, the channels for ambient backscatter communication systems are different from those for traditional point-to-point systems or cooperative relay networks since transmitting bit “0” or “1” implies backscattering or not, which leads to various channel parameters and thus dissimilar channel statistics [33]. Thirdly, signal detection at the reader is expected to be a challenging task for two reasons: (1) the ambient backscatter communication system exploits signals from other systems, which is unknown to the reader, and accordingly the reader cannot estimate the channel parameters due to lack of training symbols; (2) the signal detection at the reader is to discern backscattering or not, instead of positive or negative electrical levels or separate phases that are usually met in other existing communication systems [30]. Fourthly, performance analysis for ambient backscatter communication systems, such as BER, throughput and capacity, is to be investigated. Lastly, backscatter may produce wireless signals at the tag and hence results in the interference to legacy receivers, and thus the impact and range of the interference generated by tag to legacy receivers are to be evaluated. Meanwhile, due to broadcast nature of wireless channels, security problems [32] [31] for the tag, the reader, and also

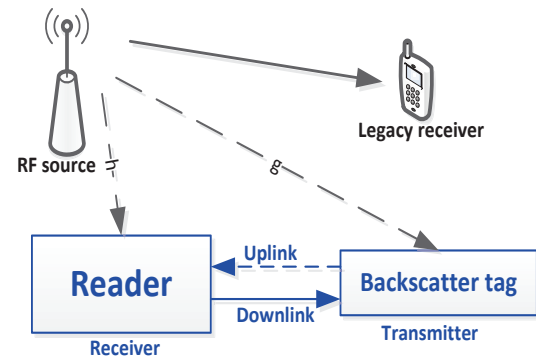


Fig. 2. A communication system of RF-powered devices that utilizes ambient backscatter.

the legacy receiver are worthy of further investigation.

In this very work, we focus on the problem of signal detection and BER performance analysis at the reader. To overcome the lack of training symbols, we adopt the differential encoder at the tag. We formulate a theoretical system model and design the data detection approach that eliminates the need for channel state information (CSI). Two detection thresholds are also proposed: one achieves approximately minimum BER while the other yields balanced error probabilities for detecting bits “0” and “1”. The corresponding BER performance is also analyzed and a simplified BER expression, as well as its upper and lower bounds are derived in high signal-to-noise ratio (SNR) region. Finally, simulation results are provided to verify the derived results.

The rest of this paper is organized as follows: Section II depicts the theoretical model for ambient backscatter communication systems with differential encoder. Section III derives the minimum BER detector and the closed-form BER expression. An approximate detection threshold for the minimum BER detector is also obtained in this section. Section IV analyzes the BER performance at high SNR and obtains both lower/upper BER bounds. The other detection threshold that can lead to equal error probabilities for detecting “0” bits and “1” bits is presented in Section V. Section VI provides simulation results and Section VII concludes the paper.

II. SYSTEM MODEL

Consider an ambient backscatter communication system with one reader and one tag, as shown in Fig. 2. Unlike conventional RFID tags, the tag here scavenges other RF signals such as TV signals [14] to communicate with the reader.

Let the RF transmit signal be $s(n)e^{j2\pi f_s n}$ where f_s is the RF carrier frequency, and $s(n)$ is the complex baseband equivalent signal. The tag receives the RF source signal and transmits its own binary signal $B(n)$ to the reader through backscattering the signal $s(n)e^{j2\pi f_s n}$ or not. Specifically, if $B(n) = 0$, the tag changes its impedance so that little energy of $s(n)$ can be reflected, while if $B(n) = 1$, the tag switches the impedance inside its circuit so that the signal can be scattered to the reader [14].

To avoid power-consuming and complexity-increasing training sequences for the battery-free tag operation [21] [22],

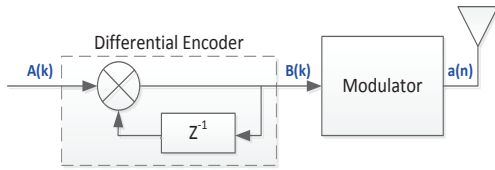


Fig. 3. Differential encoder of the backscatter tag.

and also to avoid the high BER at the reader with blind detector [23], the differential encoding is adopted at tag. That is, bit “0” corresponds to the same state in two consecutive intervals, while bit “1” corresponds to the transition from non-backscatter to backscatter or from backscatter to non-backscatter. This differential encoding is realized by a differential encoder before the modulator as shown in Fig. 3. Mathematically, the relationship between the input $A(k)$ and the output $B(k)$ of the differential encoder can be expressed as

$$B(k) = A(k) \otimes B(k-1), \quad (1)$$

where \otimes represents addition modulo 2.

Denote the channel between the RF source and the reader as h , the channel between the RF source and the tag as g , and the channel between the reader and the tag as ζ . The channels h , g , and ζ are assumed as slow-fading and remain unchanged during at least two consecutive intervals of $B(k)$. Furthermore, all these channels are unknown to the reader.

Mathematically, the signal received by the tag can be expressed as [13]

$$x(n) = gs(n)e^{j2\pi f_s n}. \quad (2)$$

Note that there may exist some carrier phase offset between the signal $x(n)$ and $s(n)$, and it can be absorbed into the complex channel g .

Moreover, the signal backscattered by the tag may be written as

$$a(n) = \eta B(n)x(n), \quad B(n) \in \{0, 1\} \quad (3)$$

where η is the complex signal attenuation inside the tag. Since the data rate of the signal $B(n)$ is much less than that of the RF signal $x(n)$, we suppose that $B(n)$ will remain unchanged within N symbols of $x(n)$. That is, $B(kN+j)$ will be the same for $j = 1, 2, \dots, N$.

Therefore, the reader receives the passband signal

$$\tilde{y}(n) = hs(n)e^{j2\pi f_s n} + \zeta a(n) + \tilde{w}_b(n), \quad (4)$$

where $\tilde{w}_b(n)$ is the zero-mean additive white Gaussian noise (AWGN) with variance N_{wb} .

Define the carrier frequency of the reader as f_r and the carrier phase offset between the RF source and the reader as θ_0 . After demodulating the received passband signal $\tilde{y}(n)$ with the carrier signal $e^{-j(2\pi f_r n + \theta_0)}$, we obtain the baseband signal as

$$\begin{aligned} y(n) &= \tilde{y}(n)e^{-j(2\pi f_r n + \theta_0)} \\ &= hs(n)e^{-j(2\pi \Delta_f n + \theta_0)} \\ &\quad + \eta \zeta g B(n)s(n)e^{-j(2\pi \Delta_f n + \theta_0)} + w_b(n), \end{aligned} \quad (5)$$

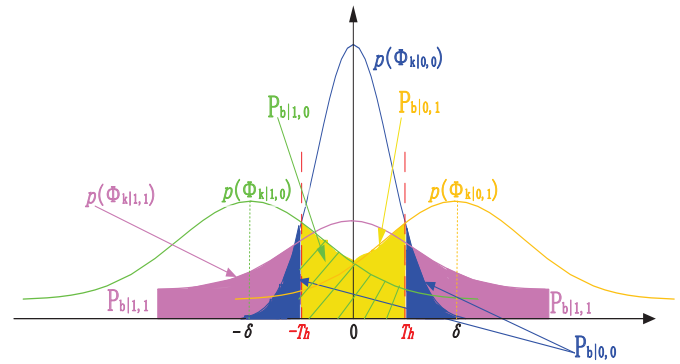


Fig. 4. PDFs of conditional random variables $\Phi_{k|0,0}$, $\Phi_{k|1,1}$, $\Phi_{k|0,1}$ and $\Phi_{k|1,0}$, and BER regions for small and positive δ .

where $\Delta_f = f_s - f_r$ is the carrier frequency offset (CFO) and $w_b(n) = \tilde{w}_b(n)e^{-j(2\pi f_r n + \theta_0)}$ is an equivalent noise with the same variance N_{wb} .

The main task of the reader is to recover $B(n)$ from the baseband signal $y(n)$ without any CSI and CFO knowledge. Note that the ambient backscatter communication system (Fig. 2) differs from traditional point-to-point and relay communication systems since $B(n)$ is hidden in $y(n)$. Consequently, a specific detection method must be designed to recover $B(n)$.

Remark 1: Following the analysis in [12], the signal (4) can also be modeled as

$$\tilde{y}(n) = hs(n)e^{j2\pi f_s n} + \zeta a(n) + \zeta \tilde{w}_a(n) + \tilde{w}_b(n), \quad (6)$$

where $\tilde{w}_a(n)$ denotes the AWGN term at the tag and is sent back to the reader. Nevertheless, the tag circuit consists only of passive components and takes few signal processing operations, the thermal noise is usually negligible, i.e., $\tilde{w}_a(n) \approx 0$. A detailed analysis about the backscattered radiated field and the channel modeling can be found in [25], [5], [13].

Remark 2: Strictly speaking, the signal received by the reader should be $\tilde{y}(n) = hs(n)e^{j2\pi f_s n} + \zeta a(n - \tau) + \tilde{w}_b(n)$, where τ represents the time delay from the tag to the reader. The time delay τ consists of two parts: the delay inside the circuit of the tag and the delay caused by the distance from the tag to the reader. However, the time delay τ can be ignored in backscattering systems because: (i) The electrical signal inside the circuit of the tag and the electromagnetic wave travel as fast as the speed of light; (ii) The communication range of RF-powered devices are limited, currently being less than 130 meters [13]. Hence, τ is usually much less than one symbol intervals of $s(n)$ and can be ignored.

III. SIGNAL DETECTION AT THE READER

Let us rewrite (5) as

$$y(n) = \begin{cases} hs(n)e^{-j(2\pi \Delta_f n + \theta_0)} + w_b(n), & B(n) = 0 \\ \mu s(n)e^{-j(2\pi \Delta_f n + \theta_0)} + w_b(n), & B(n) = 1 \end{cases} \quad (7)$$

where $\mu \triangleq h + \eta \zeta g$ denotes the combined channel information.

Suppose KN signal samples are available to the reader. We then compute the average power of the N samples of $y(n)$ that

correspond to each single backscattered bit as

$$\Gamma_k = \frac{1}{N} \sum_{n=(k-1)N+1}^{kN} |y(n)|^2, \quad 1 \leq k \leq K. \quad (8)$$

It can be easily found that

$$\Gamma_k = \begin{cases} \Gamma_{k,0} = M_{k,0} + L_{k,0}, & B(n) = 0 \\ \Gamma_{k,1} = M_{k,1} + L_{k,1}, & B(n) = 1 \end{cases} \quad (9)$$

where

$$M_{k,0} = \sum_{n=(k-1)N+1}^{kN} \frac{|h|^2 |s(n)|^2 + |w_b(n)|^2}{N}, \quad (10)$$

$$M_{k,1} = \sum_{n=(k-1)N+1}^{kN} \frac{|\mu|^2 |s(n)|^2 + |w_b(n)|^2}{N}, \quad (11)$$

$$L_{k,0} = \frac{1}{N} \sum_{n=(k-1)N+1}^{kN} 2\Re \left\{ h s(n) e^{-j(2\pi\Delta_f n + \theta_0)} w_b^H(n) \right\}, \quad (12)$$

$$L_{k,1} = \frac{1}{N} \sum_{n=(k-1)N+1}^{kN} 2\Re \left\{ \mu s(n) e^{-j(2\pi\Delta_f n + \theta_0)} w_b^H(n) \right\}. \quad (13)$$

Assuming that the slow-fading channels h , ζ and g remain unchanged during some consecutive intervals of transmitting $B(k-1)$ and $B(k)$, the central limit theorem (CLT) [26] yields that $L_{k,0} \sim \mathcal{N}(0, \varsigma_0^2)$ and $L_{k,1} \sim \mathcal{N}(0, \varsigma_1^2)$, with

$$\varsigma_0^2 = \frac{2}{N} |h|^2 P_s N_{wb}, \quad \varsigma_1^2 = \frac{2}{N} |\mu|^2 P_s N_{wb}, \quad (14)$$

where P_s is the average power of $s(n)$ that is unknown to the reader.

A. Large N Case

When N is a large number, the following approximations can be made:

$$M_{k,0} \approx |h|^2 P_s + N_{wb}, \quad (15)$$

$$M_{k,1} \approx |\mu|^2 P_s + N_{wb}. \quad (16)$$

Therefore, we obtain

$$\Gamma_k = \begin{cases} \Gamma_{k,0} \sim \mathcal{N}(|h|^2 P_s + N_{wb}, \varsigma_0^2), \\ \Gamma_{k,1} \sim \mathcal{N}(|\mu|^2 P_s + N_{wb}, \varsigma_1^2). \end{cases} \quad (17)$$

B. Small N Case

When N is a small number, $M_{k,0}$ and $M_{k,1}$ can be considered as Gaussian distributed random variables instead of constants,

$$M_{k,0} \sim \mathcal{N}\left(|h|^2 P_s + N_{wb}, \frac{N_{wb}^2}{N}\right), \quad (18)$$

$$M_{k,1} \sim \mathcal{N}\left(|\mu|^2 P_s + N_{wb}, \frac{N_{wb}^2}{N}\right). \quad (19)$$

Therefore, we obtain

$$\Gamma_k = \begin{cases} \Gamma_{k,0} \sim \mathcal{N}(|h|^2 P_s + N_{wb}, \sigma_0^2), \\ \Gamma_{k,1} \sim \mathcal{N}(|\mu|^2 P_s + N_{wb}, \sigma_1^2), \end{cases} \quad (20)$$

where

$$\sigma_0^2 = \frac{N_{wb}^2}{N} + \varsigma_0^2, \quad \sigma_1^2 = \frac{N_{wb}^2}{N} + \varsigma_1^2. \quad (21)$$

It can be found that the expression Γ_k (20) for the small N case is similar to (17) for the large N case except for different variances. Hence, we next only present the detection approach and the BER analysis for the large N case, and the corresponding discussions for small N case can be similarly obtained.

C. Minimum BER Detector

Since no CSI is available, we will design the data detector utilizing the difference²

$$\Phi_k = \Gamma_k - \Gamma_{k-1}. \quad (22)$$

Our goal is to design an optimal detector that can minimize the error probability, or equivalently, maximize the correct probability

$$\begin{aligned} \hat{A}(k) &= \arg \max_{A(k) \in \{0,1\}} \Pr(\text{correct decision} | \Phi_k) \\ &= \arg \max_{A(k) \in \{0,1\}} \Pr(A(k) | \Phi_k). \end{aligned} \quad (23)$$

According to Bayes' rule, we can write (23) as

$$\hat{A}(k) = \arg \max_{A(k) \in \{0,1\}} \frac{\Pr(\Phi_k | A(k)) \Pr(A(k))}{\Pr(\Phi_k)}. \quad (24)$$

Since the transmit messages $A(k) = 0$ and $A(k) = 1$ are equiprobable, we can further simplify (24) as

$$\hat{A}(k) = \arg \max_{A(k) \in \{0,1\}} \Pr(\Phi_k | A(k)). \quad (25)$$

The detectors (23) and (25) are well-known as *maximum a posteriori probability* (MAP) receiver and *maximum-likelihood* (ML) receiver respectively.

Since the tag uses differential encoding, the message $A(k) = 0$ (or $A(k) = 1$) can be fully determined by $B(k)$ and $B(k-1)$. For the cases $B(k-1) = B(k)$ that indicates $A(k) = 0$, we can further compute Φ_k as

$$\Phi_k = \begin{cases} \Phi_{k|0,0} = L_{k,0} - L_{k-1,0}, & B(k-1) = B(k) = 0 \\ \Phi_{k|1,1} = L_{k,1} - L_{k-1,1}, & B(k-1) = B(k) = 1 \end{cases} \quad (26)$$

It can be readily checked that $\Phi_{k|0,0} \sim \mathcal{N}(0, 2\varsigma_0^2)$ and $\Phi_{k|1,1} \sim \mathcal{N}(0, 2\varsigma_1^2)$.

For the cases $B(k-1) \neq B(k)$ that indicates $A(k) = 1$, we can compute Φ_k as

$$\begin{aligned} \Phi_k &= \quad (27) \\ \begin{cases} \Phi_{k|0,1} = \delta + L_{k,1} - L_{k-1,0}, & B(k-1) = 0, B(k) = 1 \\ \Phi_{k|1,0} = -\delta + L_{k,0} - L_{k-1,1}, & B(k-1) = 1, B(k) = 0 \end{cases} \end{aligned}$$

where

$$\delta = (|\mu|^2 - |h|^2) P_s. \quad (28)$$

²Different from the conventional differential detector where the division between the two consecutive symbols is used, we here resort to the difference between the two consecutive symbols due to the new structure of ambient backscatter systems.

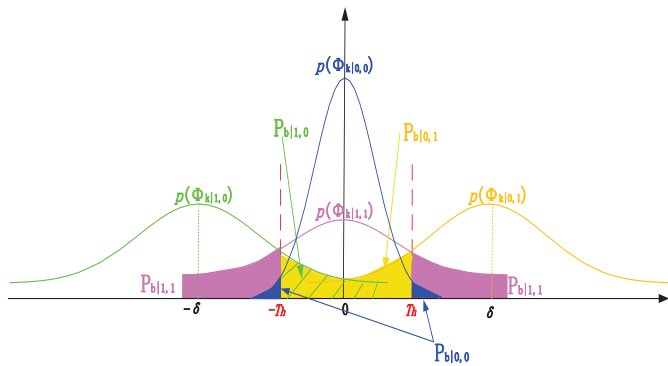


Fig. 5. PDFs of $p(\Phi_{k|0,0})$, $p(\Phi_{k|1,1})$, $p(\Phi_{k|0,1})$ and $p(\Phi_{k|1,0})$, and BER regions for large and positive δ .

Clearly, $\Phi_{k|0,1} \sim \mathcal{N}(\delta, \zeta_0^2 + \zeta_1^2)$ and $\Phi_{k|1,0} \sim \mathcal{N}(-\delta, \zeta_0^2 + \zeta_1^2)$.

Let $p(\Phi_{k|0,0})$, $p(\Phi_{k|1,1})$, $p(\Phi_{k|0,1})$ and $p(\Phi_{k|1,0})$ denote the probability density functions (PDFs) of the conditional random variables $\Phi_{k|0,0}$, $\Phi_{k|1,1}$, $\Phi_{k|0,1}$ and $\Phi_{k|1,0}$ that are Gaussian distributed. Note that due to the randomness of the channel gains $|h|^2$ and $|\mu|^2$, the values of δ can be either small or large, either positive or negative, and therefore these PDFs vary at different transmission slots, which imposes more difficulty in signal detection for the reader.

Fig. 4 shows the PDFs of the conditional random variables $\Phi_{k|0,0}$, $\Phi_{k|1,1}$, $\Phi_{k|0,1}$ and $\Phi_{k|1,0}$ in case of small and positive δ . The corresponding BER regions of $P_{b|0,0}$, $P_{b|1,1}$, $P_{b|0,1}$ and $P_{b|1,0}$ are given in blue, purple, yellow and green shadowed part separately. Fig. 5 show the same PDFs and BER regions for large and positive δ .

As shown in Fig. 4, if Φ_k falls into the region around zero, then we know $p(\Phi_{k|0,0}) > p(\Phi_{k|1,0})$ or $p(\Phi_{k|0,0}) > p(\Phi_{k|0,1})$, which indicates the optimal decision will be $\hat{A}(k) = 0$; If Φ_k falls into the region around δ or larger than δ , then $p(\Phi_{k|1,1}) < p(\Phi_{k|1,0})$ or $p(\Phi_{k|1,1}) < p(\Phi_{k|0,1})$ holds, which says the optimal decision will be $\hat{A}(k) = 1$.

Define

$$p_0(x) = \Pr(\Phi_k | A(k) = 0), \quad (29)$$

$$p_1(x) = \Pr(\Phi_k | A(k) = 1). \quad (30)$$

Since

$$\Pr(A(k) = 0) = \Pr(B(k-1) = B(k) = 1) + \Pr(B(k-1) = B(k) = 0), \quad (31)$$

$$\Pr(A(k) = 1) = \Pr(B(k-1) = 0, B(k) = 1) + \Pr(B(k-1) = 1, B(k) = 0), \quad (32)$$

we have

$$p_0(x) = \frac{1}{2} (p(\Phi_{k|0,0}) + p(\Phi_{k|1,1})) = \frac{1}{4\sqrt{\pi\zeta_0^2}} e^{-\frac{x^2}{4\zeta_0^2}} + \frac{1}{4\sqrt{\pi\zeta_1^2}} e^{-\frac{x^2}{4\zeta_1^2}}, \quad (33)$$

$$p_1(x) = \frac{1}{2} (p(\Phi_{k|0,1}) + p(\Phi_{k|1,0})) = \frac{1}{\sqrt{8\pi\zeta_+^2}} e^{-\frac{(x-\delta)^2}{2\zeta_+^2}} + \frac{1}{\sqrt{8\pi\zeta_+^2}} e^{-\frac{(x+\delta)^2}{2\zeta_+^2}}, \quad (34)$$

where $\zeta_+^2 = \zeta_0^2 + \zeta_1^2$.

Subsequently, our ML detection rule (25) can be reformulated as

$$\begin{cases} \hat{A}(k) = 0, & \text{if } p_0(x) > p_1(x), \\ \hat{A}(k) = 1, & \text{if } p_0(x) < p_1(x). \end{cases} \quad (35)$$

The ML decision rule is: decode $\hat{A}(k) = 0$ when $0 \leq |\Phi_k| < T_h$, and $\hat{A}(k) = 1$ otherwise. Here, T_h represents a properly chosen threshold.

D. ML Decision Regions

Clearly, the optimal threshold T_h^{opt} for the ML detector should satisfy

$$p_0(x) = p_1(x) \Big|_{x=T_h^{opt}}. \quad (36)$$

Unfortunately, closed-form solution for (36) does not exist. Therefore, we resort to approximate solutions through the following theorem.

Theorem 1: The solution for (36) can be approximated by

$$T_h^{app} = \frac{|\delta|}{2} + \frac{\zeta_+^2}{|\delta|} \ln \left(1 + \sqrt{1 - e^{-\delta^2/\zeta_+^2}} \right). \quad (37)$$

Proof: See Appendix A. ■

Remark 3: Since the channel information such as h , μ , $|h|^2$ and $|\mu|^2$ is not available at the reader, neither the optimal threshold T_h^{opt} nor the approximate threshold T_h^{app} can be calculated by the detector. To solve this problem, we derive another practical substitution at high SNR, which will be introduced in the next Section.

E. BER Performance

Given threshold T_h , the BER for the ML detector can be expressed as

$$P_b = \Pr(A(k) = 1) \Pr(\hat{A}(k) = 0 | A(k) = 1) + \Pr(A(k) = 0) \Pr(\hat{A}(k) = 1 | A(k) = 0). \quad (38)$$

It can be further found that

$$\Pr(\hat{A}(k) = 0 | A(k) = 1) = \frac{1}{2} P_{b|0,0} + \frac{1}{2} P_{b|1,1}, \quad (39)$$

where

$$P_{b|0,0} = \Pr(\hat{A}(k) = 1 | B(k-1) = 0, B(k) = 0) = 1 - \int_{-T_h}^{T_h} p(\Phi_{k|0,0}) d\Phi_{k|0,0} = 2Q \left(\frac{T_h}{\sqrt{2\zeta_0^2}} \right), \quad (40)$$

$$P_{b|1,1} = \Pr(\hat{A}(k) = 1 | B(k-1) = 1, B(k) = 1), = 1 - \int_{-T_h}^{T_h} p(\Phi_{k|1,1}) d\Phi_{k|1,1}, = 2Q \left(\frac{T_h}{\sqrt{2\zeta_1^2}} \right), \quad (41)$$

and the Q function, which is the Gaussian tail probability, is defined as

$$Q(x) = \frac{1}{\sqrt{2\pi}} \int_x^\infty e^{-\frac{t^2}{2}} dt. \quad (42)$$

Similarly, we can obtain

$$\Pr(\hat{A}(k) = 1 | A(k) = 0) = \frac{1}{2} P_{b|0,1} + \frac{1}{2} P_{b|1,0}, \quad (43)$$

where

$$\begin{aligned} P_{b|0,1} &= \Pr(\hat{A}(k) = 0 | B(k-1) = 0, B(k) = 1) \\ &= \int_{-T_h}^{T_h} p(\Phi_{k|0,1}) d\Phi_{k|0,1} \\ &= Q\left(\frac{-T_h - \delta}{\sqrt{\zeta_0^2 + \zeta_1^2}}\right) - Q\left(\frac{T_h - \delta}{\sqrt{\zeta_0^2 + \zeta_1^2}}\right), \end{aligned} \quad (44)$$

$$\begin{aligned} P_{b|1,0} &= \Pr(\hat{A}(k) = 0 | B(k-1) = 1, B(k) = 0) \\ &= \int_{-T_h}^{T_h} p(\Phi_{k|1,0}) d\Phi_{k|1,0} \\ &= Q\left(\frac{-T_h + \delta}{\sqrt{\zeta_0^2 + \zeta_1^2}}\right) - Q\left(\frac{T_h + \delta}{\sqrt{\zeta_0^2 + \zeta_1^2}}\right). \end{aligned} \quad (45)$$

It can be readily checked that $P_{b|0,1} = P_{b|1,0}$ due to symmetry. Therefore, substituting (40), (41), (44) and (45) into (38), we can obtain the BER expression as

$$\begin{aligned} P_b &= \frac{1}{2}Q\left(\frac{T_h}{\sqrt{2\zeta_0^2}}\right) + \frac{1}{2}Q\left(\frac{T_h}{\sqrt{2\zeta_1^2}}\right) \\ &+ \frac{1}{2}Q\left(\frac{-T_h + \delta}{\sqrt{\zeta_0^2 + \zeta_1^2}}\right) - \frac{1}{2}Q\left(\frac{T_h + \delta}{\sqrt{\zeta_0^2 + \zeta_1^2}}\right). \end{aligned} \quad (46)$$

Remark 4: Based on the derived instantaneous BER expression (46), the average BER \bar{P}_b can be calculated or simulated through statistical mean over all channel realizations.

IV. PERFORMANCE AT HIGH SNR

At high SNR region, we could achieve much concise results as opposed to those in the previous section.

A. Approximate Optimal Threshold

Theorem 2: At high SNR, the optimal threshold T_h^{opt} can be approximated by $E(|\Phi_k|)$ in the case of large K .

Proof: In high SNR, the first item in (37) is much larger than the second one. Therefore, $T_h^{opt} \approx |\delta|/2$. Combining the fact that $E(|\Phi_k|) \approx |\delta|/2$ when K is relatively large, we know the threshold T_h^{opt} can be approximated as $E(|\Phi_k|)$. ■

Obviously, $E(|\Phi_k|)$ can be practically achieved at the reader after receiving a sequence of (8) and calculating (22).

B. Upper and Lower Bounds for BER

At high SNR, if we take $T_h = |\delta|/2$, then there are

$$P_{b|0,0} = 2Q\left(\frac{|\delta|/2}{\sqrt{2\zeta_0^2}}\right) \approx 2Q\left(\frac{\Delta_{\mu h}}{4|h|}\sqrt{\gamma N}\right), \quad (47)$$

$$P_{b|1,1} = 2Q\left(\frac{|\delta|/2}{\sqrt{2\zeta_1^2}}\right) \approx 2Q\left(\frac{\Delta_{\mu h}}{4|\mu|}\sqrt{\gamma N}\right), \quad (48)$$

and

$$\begin{aligned} P_{b|0,1} &= Q\left(\frac{|\delta|/2}{\sqrt{\zeta_0^2 + \zeta_1^2}}\right) - Q\left(\frac{3|\delta|/2}{\sqrt{\zeta_0^2 + \zeta_1^2}}\right) = P_{b|1,0} \quad (49) \\ &\approx Q\left(\frac{\Delta_{\mu h}}{2\sqrt{2}\sqrt{\Xi_{\mu h}}}\sqrt{\gamma N}\right) - Q\left(\frac{3\Delta_{\mu h}}{2\sqrt{2}\sqrt{\Xi_{\mu h}}}\sqrt{\gamma N}\right), \end{aligned}$$

where $\gamma = P_s/N_{wb}$ and

$$\Delta_{\mu h} = ||\mu|^2 - |h|^2|, \quad \Xi_{\mu h} = |h|^2 + |\mu|^2. \quad (50)$$

The reference [28] gives a simple but good approximation for $Q(x)$

$$Q(x) \approx \frac{1}{12}e^{-\frac{x^2}{2}} + \frac{1}{4}e^{-\frac{2x^2}{3}}, \quad x > 0. \quad (51)$$

Utilizing the approximation (51) and substituting (47), (48), and (49) into (38) will produce

$$\begin{aligned} P_b|_{T_h=|\delta|/2} &\approx \quad (52) \\ &\frac{1}{24}e^{-\frac{\Delta_{\mu h}^2 \gamma N}{32|h|^2}} + \frac{1}{8}e^{-\frac{\Delta_{\mu h}^2 \gamma N}{24|h|^2}} + \frac{1}{24}e^{-\frac{\Delta_{\mu h}^2 \gamma N}{32|\mu|^2}} + \frac{1}{8}e^{-\frac{\Delta_{\mu h}^2 \gamma N}{24|\mu|^2}} \\ &+ \frac{1}{24}e^{-\frac{\Delta_{\mu h}^2 \gamma N}{16\Xi_{\mu h}}} + \frac{1}{8}e^{-\frac{\Delta_{\mu h}^2 \gamma N}{12\Xi_{\mu h}}} - \frac{1}{24}e^{-\frac{9\Delta_{\mu h}^2 \gamma N}{16\Xi_{\mu h}}} - \frac{1}{8}e^{-\frac{3\Delta_{\mu h}^2 \gamma N}{4\Xi_{\mu h}}}. \end{aligned}$$

Define

$$\Xi_l = \min(|h|^2, |\mu|^2), \quad \Xi_u = \max(|h|^2, |\mu|^2). \quad (53)$$

It can be readily checked that

$$2\Xi_l \leq \Xi_{\mu h} \leq 2\Xi_u. \quad (54)$$

Since the function $e^{-\frac{1}{x}}$ is an increasing function with x , we obtain

$$P_b|_{T_h=|\delta|/2} \leq \frac{1}{8}e^{-\frac{\Delta_{\mu h}^2 \gamma N}{32\Xi_u}} + \frac{3}{8}e^{-\frac{\Delta_{\mu h}^2 \gamma N}{24\Xi_u}} \triangleq P_{ub}, \quad (55)$$

$$P_b|_{T_h=|\delta|/2} \geq \frac{5}{48}e^{-\frac{\Delta_{\mu h}^2 \gamma N}{32\Xi_l}} + \frac{5}{16}e^{-\frac{\Delta_{\mu h}^2 \gamma N}{24\Xi_l}} \triangleq P_{lb}, \quad (56)$$

where P_{ub} and P_{lb} are defined as the corresponding upper and lower bounds of the BER P_b when the threshold is chosen as $T_h = \delta/2$, respectively.

Remark 5: It is well-known that in traditional point-to-point or cooperative communication systems, the BER performance is mainly decided by SNR and channel fading. However, in ambient backscatter communication systems, the BER is determined not only by the SNR γ and the channel fading $|h|$, $|\mu|$, but also by the channel difference $\Delta_{\mu h}$ and the number N . In addition, the BER can be considered as a decreasing function of variables γ , N and $\Delta_{\mu h}$, but as an increasing function of variables $|h|$ and $|\mu|$.

V. EQUIPROBABLE ERROR DETECTOR

The detector designed in Section III-C is optimal in that it can minimize the BER. However, this detector may not obtain the same error probability for $A(k) = 0$ and $A(k) = 1$, i.e., $\Pr(\hat{A}(k) = 1 | A(k) = 0) \neq \Pr(\hat{A}(k) = 0 | A(k) = 1)$, which is generally referred to as unbalanced BER [34].

In most practical communication process, the information bits 1 and 0 are transmitted with equal probability. Hence, the detector that achieves $\Pr(\hat{A}(k) = 1 | A(k) = 0) = \Pr(\hat{A}(k) = 0 | A(k) = 1)$ is also worth studying, i.e.,

$$P_{b|0,0} + P_{b|1,1} = P_{b|0,1} + P_{b|1,0}. \quad (57)$$

For expression simplicity, such detector is called as equiprobable error detector.

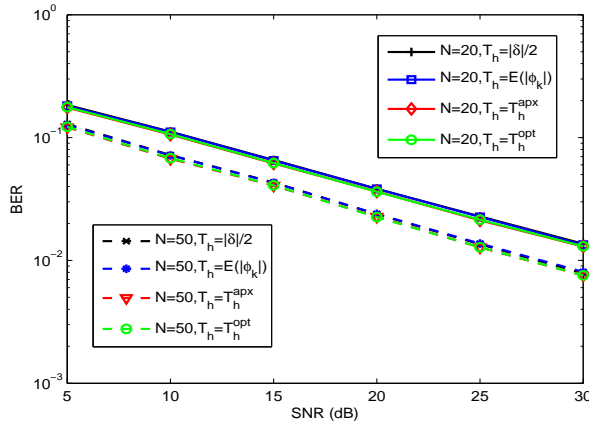


Fig. 6. BER versus transmit SNR for four different thresholds.

According to the analysis in Section III-E, and supposing $T_h = T_h^{eq}$ can satisfy the equation (57), we can further obtain

$$Q\left(\frac{T_h^{eq}}{\sqrt{2\zeta_0^2}}\right) + Q\left(\frac{T_h^{eq}}{\sqrt{2\zeta_1^2}}\right) = Q\left(\frac{-T_h^{eq} - \delta}{\sqrt{\zeta_0^2 + \zeta_1^2}}\right) - Q\left(\frac{T_h^{eq} - \delta}{\sqrt{\zeta_0^2 + \zeta_1^2}}\right). \quad (58)$$

Unfortunately, it is difficult to obtain the exact closed-form solution for T_h^{eq} in (58). We then resort to an approximation and provide the following theorem.

Theorem 3: At high SNR region, the threshold T_h^{eq} that satisfies $\Pr(\hat{A}(k) = 1|A(k) = 0) = \Pr(\hat{A}(k) = 0|A(k) = 1)$ can be approximated by

$$\tilde{T}_h^{eq} \approx \begin{cases} \frac{1}{2a} (B_e - \sqrt{B_e^2 - 4aC_e}), & |\zeta_0^2 - \zeta_1^2| \geq 1 \\ \frac{|\delta|}{2} + \frac{(\zeta_0^2 + \zeta_1^2) \ln 2}{2b\sqrt{\zeta_0^2 + \zeta_1^2} + 2a|\delta|}, & |\zeta_0^2 - \zeta_1^2| \leq 1 \end{cases} \quad (59)$$

where $b = 0.717$, $a = 0.416$, and

$$B_e = (2 + \sqrt{2})b\sqrt{\max(\zeta_0^2, \zeta_1^2)} + 4a|\delta|, \quad (60)$$

$$C_e = 2a\delta^2 + 2\max(\zeta_0^2, \zeta_1^2) \ln 2 + 2b|\delta|\sqrt{\max(\zeta_0^2, \zeta_1^2)}. \quad (61)$$

Proof: See Appendix B. ■

VI. SIMULATION RESULTS

In this section, we numerically examine the proposed studies. The noise variance N_{wb} is set as 1 and K is chosen as 100. All channels h , g , and ζ are complex Gaussian random variables with zero mean and unit variance. The complex signal attenuation inside the tag η is fixed as 1.1 dB [18].

Fig. 6 presents the BER versus SNR under four thresholds: T_h^{opt} , T_h^{apx} , $E(|\Phi_k|)$, and $|\delta|/2$. It is worth noting that only the threshold $E(|\Phi_k|)$ can be calculated in practice, and other three thresholds T_h^{opt} , T_h^{apx} , and $|\delta|/2$ are theoretically derived from the equations (36), (37), and (28), respectively. We first set the number of averaging samples N as 20 and increase the transmit SNR from 0 dB to 30 dB. For each SNR, we obtain the theoretical optimal threshold T_h^{opt} from (36) and compute the average BER after 10^4 Monte Carlo

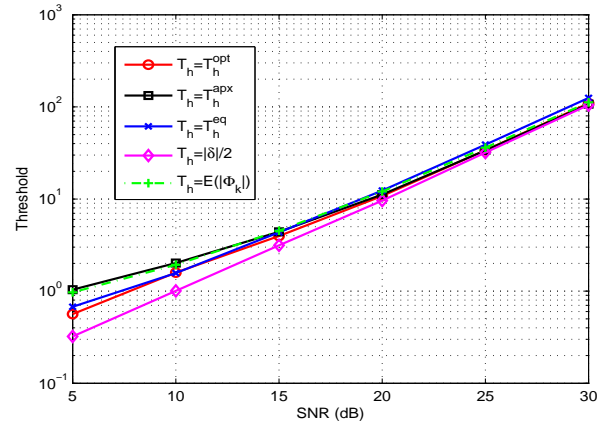


Fig. 7. Five thresholds T_h^{opt} , T_h^{apx} , T_h^{eq} , $|\delta|/2$ and $E(|\Phi_k|)$ versus SNR.

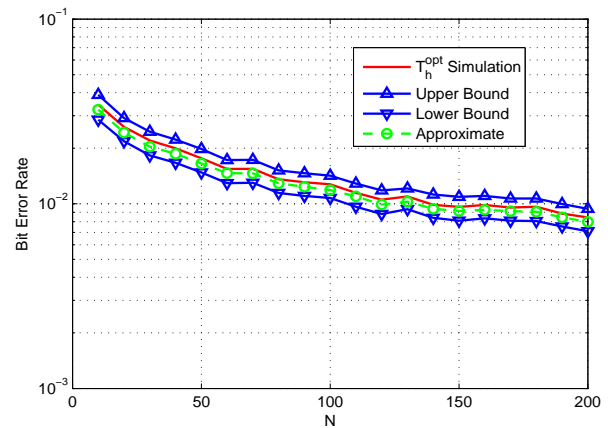


Fig. 8. BER versus N , the number of samples for averaging.

simulations. We then set the threshold as $E(|\Phi_k|)$ and obtain the simulated BER. We also set the threshold as T_h^{apx} (37) and $|\delta|/2$ (28) respectively, and find the corresponding BERs. We then set $N = 50$ and repeat the above process. It is found that the optimal threshold T_h^{opt} slightly outperforms $E(|\Phi_k|)$, T_h^{apx} and $|\delta|/2$, and the difference are slight. Moreover, though $E(|\Phi_k|)$, T_h^{apx} and $|\delta|/2$ are designed from high SNR region, their performances are also very good at low SNR region. It is also seen from Fig. 6 that larger N can lead to reduced BER, as expected.

Fig. 7 depicts the curves of five different thresholds T_h^{opt} , T_h^{apx} , T_h^{eq} , $|\delta|/2$ and $E(|\Phi_k|)$ versus SNR. At low SNR region, we see that there exists difference between T_h^{opt} and $|\delta|/2$. Nevertheless, when SNR is greater than 20dB, the difference vanishes, which agrees with Theorem 2. Besides, the value $E(|\Phi_k|)$ (or T_h^{apx} or T_h^{eq}) can be a good approximate for T_h^{opt} at high SNR, while there exists a large gap between T_h^{opt} and $E(|\Phi_k|)$ (or T_h^{apx} or T_h^{eq}) at low SNR. Nevertheless, the difference in the thresholds would not cause obvious difference in BER performance at low SNR region, as already seen in Fig. 6.

Fig. 8 shows the curves of BER versus N when SNR=30dB. The detectors choose the optimal threshold T_h^{opt} and the corresponding BER are plotted. For comparison, the

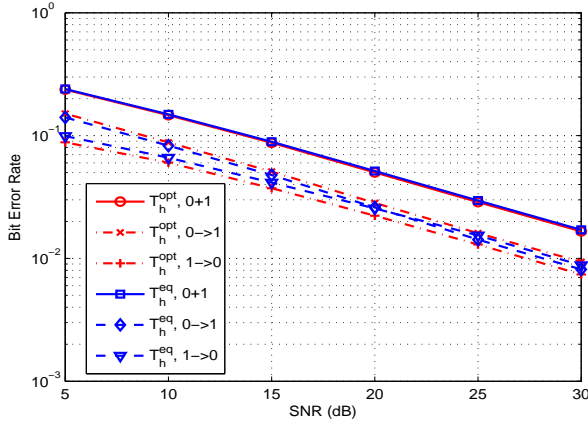


Fig. 9. BER versus SNR in the case of $T_h = T_h^{opt}$ and $T_h = T_h^{eq}$.

upper bound (56) and lower bound (55), as well as the approximate BER (52), are also plotted. Clearly, the theoretical BER approximates the simulated one very well, and the upper and lower bounds are fairly close to the simulated BER. It is seen that increasing N can quickly decrease the BER when N is small, while becomes slowly effective when N is larger, say greater than 120.

Fig. 9 presents the BER curves versus SNR when thresholds are set as T_h^{opt} and T_h^{eq} respectively. In addition, the BERs $0.5 \times \Pr[\hat{A}(k) = 1|A(k) = 0]$ and $0.5 \times \Pr[\hat{A}(k) = 0|A(k) = 1]$ are also separately plotted. It can be seen that the threshold T_h^{opt} only fractionally outperforms the threshold T_h^{eq} . More importantly, it can be found that the threshold T_h^{opt} does produce unbalanced BER, that is, $\Pr(\hat{A}(k) = 1|A(k) = 0) > \Pr(\hat{A}(k) = 0|A(k) = 1)$. Nevertheless, the derived threshold T_h^{eq} can reduce the gap between $\Pr(\hat{A}(k) = 1|A(k) = 0)$ and $\Pr(\hat{A}(k) = 0|A(k) = 1)$, especially at high SNR region.

VII. CONCLUSION

Ambient backscatter is an emerging wireless communication technology that offers a large market potential as well as many open research problems. In this paper, we developed a theoretical model for such communication links with a differential encoder for the tag. Furthermore, we derived both minimum-BER detector and the optimal detection threshold. We also derived BER expressions and both upper and lower closed-form BER bounds. In addition, an equiprobable error detector and the corresponding detection threshold were designed to obtain balanced BER. Finally, simulation results were provided to corroborate our theoretical results.

APPENDIX A

PROOF OF THEOREM 1

The function $p_0(x)$ of the two PDFs' sum can be approximated by

$$\tilde{p}_0(x) = \frac{1}{\sqrt{2\pi\zeta_+^2}} e^{-\frac{x^2}{2\zeta_+^2}}. \quad (\text{A.1})$$

Fig. 10 illustrates the approximation where $\zeta_1^2 = 2\zeta_0^2$.

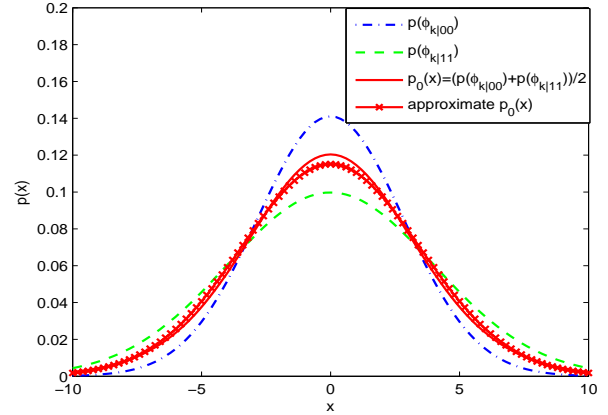


Fig. 10. Approximate expression for $p_0(x)$.

We can then rewrite (36) as

$$2e^{-\frac{x^2}{2\zeta_+^2}} = e^{-\frac{(x-\delta)^2}{2\zeta_+^2}} + e^{-\frac{(x+\delta)^2}{2\zeta_+^2}}, \quad (\text{A.2})$$

which can be further simplified as

$$e^{\frac{x\delta}{\zeta_+^2}} + e^{-\frac{x\delta}{\zeta_+^2}} = 2e^{\frac{\delta^2}{2\zeta_+^2}}. \quad (\text{A.3})$$

Treating the whole element $e^{\frac{x\delta}{\zeta_+^2}}$ as a variable, we can obtain from (A.3)

$$e^{\frac{x\delta}{\zeta_+^2}} = \begin{cases} e^{\frac{\delta^2}{2\zeta_+^2}} + \sqrt{e^{\frac{\delta^2}{\zeta_+^2}} - 1}, & \delta > 0 \\ e^{\frac{\delta^2}{2\zeta_+^2}} - \sqrt{e^{\frac{\delta^2}{\zeta_+^2}} - 1}, & \delta < 0. \end{cases} \quad (\text{A.4})$$

Note that (A.4) can be rewritten as

$$e^{\frac{\delta^2}{2\zeta_+^2}} + \sqrt{e^{\frac{\delta^2}{\zeta_+^2}} - 1} = \begin{cases} e^{\frac{x\delta}{\zeta_+^2}}, & \delta > 0 \\ e^{-\frac{x\delta}{\zeta_+^2}}, & \delta < 0 \end{cases} \quad (\text{A.5})$$

Taking logarithm operations for both sides of (A.5) yields

$$x = \begin{cases} \frac{\delta}{2} + \frac{\zeta_+^2}{\delta} \ln\left(1 + \sqrt{1 - e^{-\delta^2/\zeta_+^2}}\right), & \delta > 0 \\ -\frac{\delta}{2} - \frac{\zeta_+^2}{\delta} \ln\left(1 + \sqrt{1 - e^{-\delta^2/\zeta_+^2}}\right), & \delta < 0 \end{cases} \quad (\text{A.6})$$

which proves (37).

APPENDIX B

PROOF OF THEOREM 3

At high SNR region, in the case of $\delta > 0$, we can assume $|\mu|^2 > |h|^2$ and therefore $\zeta_1^2 - \zeta_0^2 > 0$.

If $\zeta_1^2 - \zeta_0^2 \geq 1$ we have the approximation

$$\begin{aligned} P_{b|0,0} + P_{b|1,1} &\leq Q\left(\frac{T_h}{\sqrt{2\zeta_1^2}}\right), \\ P_{b|0,1} + P_{b|1,0} &\approx \frac{1}{2} - \frac{1}{2}Q\left(\frac{T_h - \delta}{\sqrt{\zeta_0^2 + \zeta_1^2}}\right) \\ &= \frac{1}{2}Q\left(\frac{\delta - T_h}{\sqrt{\zeta_0^2 + \zeta_1^2}}\right) \geq \frac{1}{2}Q\left(\frac{\delta - T_h}{\sqrt{\zeta_1^2}}\right). \end{aligned}$$

Using (57) we know that T_h^{eq} should satisfy

$$Q\left(\frac{T_h^{eq}}{\sqrt{2\zeta_1^2}}\right) \geq \frac{1}{2}Q\left(\frac{\delta - T_h^{eq}}{\sqrt{\zeta_1^2}}\right). \quad (\text{B.1})$$

Letting \tilde{T}_h^{eq} reach the equality of (B.1) and utilizing the following approximation [29] for Q function

$$Q(x) \approx \frac{1}{2}e^{-bx-ax^2}, \quad b = 0.717, a = 0.416, \quad (\text{B.2})$$

we can further obtain

$$\ln 2 - \frac{b\tilde{T}_h^{eq}}{\sqrt{2\zeta_1^2}} - \frac{a(\tilde{T}_h^{eq})^2}{2\zeta_1^2} = -\frac{b(\delta - \tilde{T}_h^{eq})}{\sqrt{\zeta_1^2}} - \frac{a(\delta - \tilde{T}_h^{eq})^2}{\zeta_1^2}, \quad (\text{B.3})$$

which can be simplified as

$$a(\tilde{T}_h^{eq})^2 - B_{e1}\tilde{T}_h^{eq} + C_{e1} = 0, \quad (\text{B.4})$$

where

$$B_{e1} = (2 + \sqrt{2})b\sqrt{\zeta_1^2} + 4a\delta, \quad (\text{B.5})$$

$$C_{e1} = 2a\delta^2 + 2\zeta_1^2 \ln 2 + 2b\delta\sqrt{\zeta_1^2}. \quad (\text{B.6})$$

The solution to (B.4) can be obtained as

$$\tilde{T}_h^{eq} = \frac{1}{2a} \left(B_{e1} - \sqrt{B_{e1}^2 - 4aC_{e1}} \right). \quad (\text{B.7})$$

On the other hand, if $0 < \zeta_1^2 - \zeta_0^2 < 1$ we have the following approximation

$$P_{b|0,0} + P_{b|1,1} \approx Q\left(\frac{T_h}{\sqrt{\zeta_0^2 + \zeta_1^2}}\right),$$

$$P_{b|0,1} + P_{b|1,0} \approx \frac{1}{2}Q\left(\frac{\delta - T_h}{\sqrt{\zeta_0^2 + \zeta_1^2}}\right).$$

According to (57) we obtain

$$2Q\left(\frac{\tilde{T}_h^{eq}}{\sqrt{\zeta_0^2 + \zeta_1^2}}\right) = Q\left(\frac{\delta - \tilde{T}_h^{eq}}{\sqrt{\zeta_0^2 + \zeta_1^2}}\right). \quad (\text{B.8})$$

Utilizing the approximation (B.2) for Q function, we can further simplify (B.8) as

$$2e^{-\frac{b\tilde{T}_h^{eq}}{\sqrt{\zeta_0^2 + \zeta_1^2}} - \frac{a(\tilde{T}_h^{eq})^2}{\zeta_0^2 + \zeta_1^2}} = e^{-\frac{b(\delta - \tilde{T}_h^{eq})}{\sqrt{\zeta_0^2 + \zeta_1^2}} - \frac{a(\delta - \tilde{T}_h^{eq})^2}{\zeta_0^2 + \zeta_1^2}}. \quad (\text{B.9})$$

The solution to (B.9) can be found as

$$\tilde{T}_h^{eq} = \frac{(\zeta_0^2 + \zeta_1^2) \ln 2 + a\delta^2 + b\sqrt{\zeta_0^2 + \zeta_1^2}\delta}{2b\sqrt{\zeta_0^2 + \zeta_1^2} + 2a\delta}. \quad (\text{B.10})$$

Similarly, in the case of $\delta < 0$, we can assume $\zeta_0^2 - \zeta_1^2 > 0$. In the case of $\zeta_0^2 - \zeta_1^2 \geq 1$, we obtain

$$P_{b|0,0} + P_{b|1,1} \leq Q\left(\frac{T_h}{\sqrt{2\zeta_0^2}}\right),$$

$$P_{b|0,1} + P_{b|1,0} = \frac{1}{2}Q\left(\frac{-T_h - \delta}{\sqrt{\zeta_0^2 + \zeta_1^2}}\right) - \frac{1}{2}Q\left(\frac{T_h - \delta}{\sqrt{\zeta_0^2 + \zeta_1^2}}\right)$$

$$\approx \frac{1}{2}Q\left(\frac{-T_h - \delta}{\sqrt{\zeta_0^2 + \zeta_1^2}}\right) \geq \frac{1}{2}Q\left(\frac{-T_h - \delta}{\sqrt{\zeta_0^2}}\right),$$

and thus

$$Q\left(\frac{T_h}{\sqrt{2\zeta_0^2}}\right) \geq \frac{1}{2}Q\left(\frac{-T_h - \delta}{\sqrt{\zeta_0^2}}\right). \quad (\text{B.11})$$

Let \tilde{T}_h^{eq} reach the equality of (B.11), we can obtain

$$a(\tilde{T}_h^{eq})^2 - B_{e2}\tilde{T}_h^{eq} + C_{e2} = 0, \quad (\text{B.12})$$

where

$$B_{e2} = (2 + \sqrt{2})b\sqrt{\zeta_0^2} - 4a\delta, \quad (\text{B.13})$$

$$C_{e2} = 2a\delta^2 + 2\zeta_0^2 \ln 2 - 2b\delta\sqrt{\zeta_0^2}. \quad (\text{B.14})$$

Subsequently, we derive the solution to (B.12) as

$$\tilde{T}_h^{eq} = \frac{1}{2a} \left(B_{e2} - \sqrt{B_{e2}^2 - 4aC_{e2}} \right). \quad (\text{B.15})$$

In the case of $1 > \zeta_0^2 - \zeta_1^2 > 0$, we have the following results

$$P_{b|0,0} + P_{b|1,1} \approx Q\left(\frac{T_h}{\sqrt{\zeta_0^2 + \zeta_1^2}}\right), \quad (\text{B.16})$$

$$P_{b|0,1} + P_{b|1,0} \approx \frac{1}{2}Q\left(\frac{-T_h - \delta}{\sqrt{\zeta_0^2 + \zeta_1^2}}\right). \quad (\text{B.17})$$

Substituting (B.16) and (B.17) into (57) and utilizing (B.2), we can find

$$\tilde{T}_h^{eq} = \frac{(\zeta_0^2 + \zeta_1^2) \ln 2 + a\delta^2 - b\sqrt{\zeta_0^2 + \zeta_1^2}\delta}{2b\sqrt{\zeta_0^2 + \zeta_1^2} - 2a\delta}. \quad (\text{B.18})$$

Combining (B.7) and (B.15) for $|\zeta_1^2 - \zeta_0^2| \geq 1$ case, and combining (B.10) and (B.18) for $0 < |\zeta_1^2 - \zeta_0^2| < 1$ case will produce (59).

REFERENCES

- [1] L. Xie, Y. Yin, A. V. Vasilakos, and S. Lu, "Managing RFID data: challenges, opportunities and solutions," *IEEE Commun. Surveys and Tutorials*, vol. 16, no. 3, pp. 1294-1311, Aug. 2014.
- [2] Idtechex. "RFID Forecasts, Players and Opportunities 2014-2024," July 2014. [Online]. Available: <http://www.idtechex.com/research/reports/rfid-forecasts-players-and-opportunities-2014-2024-000368.asp>
- [3] D. M. Dobkin, *The RF in RFID: Passive UHF RFID in Practice*. Newnes (Elsevier), 2008.
- [4] H. Stockman, "Communication by means of reflected power," *Proc. IRE*, pp. 1196-1204, Oct. 1948.
- [5] C. Boyer and S. Roy, "Backscatter communication and RFID: coding, energy and MIMO analysis," *IEEE Trans. Commun.*, vol. 62, no.3, pp. 770-785, Mar. 2014.
- [6] J. D. Griffin and G. D. Durgin, "Complete link budgets for backscatter radio and RFID systems," *IEEE Antennas Propagat. Mag.*, vol. 51, no. 2, pp. 11-25, Apr. 2009.
- [7] D. Kim, M. A. Ingram, and W. W. Smith Jr., "Measurements of small-scale fading and path loss for long range RF tags," *IEEE Trans. Antennas Propag.*, vol. 51, no. 8, pp. 1740-1749, Aug. 2003.
- [8] J. D. Griffin and G. D. Durgin, "Gains for RF tags using multiple antennas," *IEEE Trans. Antennas Propag.*, vol. 56, no. 2, pp. 563-570, Feb. 2008.
- [9] J. D. Griffin and G. D. Durgin, "Multipath fading measurement at 5.8GHz for backscatter tags with multiple antennas," *IEEE Trans. Antennas Propag.*, vol. 58, no. 11, pp. 3694-3700, Nov. 2010.
- [10] G. Vannucci, A. Bletsas, and D. Leigh, "A software-defined radio system for backscatter sensor networks," *IEEE Trans. Wireless Commun.*, vol. 2, no. 6, pp. 2170-2179, June 2008.
- [11] J. Hermans, R. Peeters, and B. Preneel, "Proper RFID privacy: model and protocols," *IEEE Trans. Mobile Computing*, vol. 13, no. 12, pp.2888-2902, Dec. 2014.

- [12] W. Saad, X. Zhou, Z. Han, and H. V. Poor, "On the physical layer security of backscatter wireless systems," *IEEE Trans. Wireless Commun.*, vol. 13, no. 6, pp. 3442-3451, Jun. 2014.
- [13] J. Kimionis, A. Bletsas, and J. N. Sahalos, "Increased range bistatic scatter radio," *IEEE Trans. Commun.*, vol. 62, no. 3, pp. 1091-1104, Mar. 2014.
- [14] V. Liu, A. Parks, V. Talla, S. Gollakota, D. Wetherall, and J. R. Smith, "Ambient backscatter: wireless communication out of thin air," in *Proc. ACM SIGCOMM*, Hong Kong, China, 2013, pp. 1-13.
- [15] B. Kellogg, A. Parks, S. Gollakota, J. R. Smith, and D. Wetherall, "Wi-Fi Backscatter: Internet connectivity for RF-powered devices," in *Proc. ACM SIGCOMM*, Chicago, USA, 2014, pp. 1-12.
- [16] D. Bharadia, K. Joshi, M. Kotaru, and S. Katti, "BackFi: high throughput WiFi backscatter," in *Proc. ACM SIGCOMM*, London, United Kingdom, 2015, pp. 283-296.
- [17] V. Iyer, V. Talla, B. Kellogg, S. Gollakota, and J. R. Smith, "Inter-Technology backscatter: towards Internet connectivity for implanted Devices," in *Proc. ACM SIGCOMM*, Florianopolis, Brazil, 2016, pp. 1-14.
- [18] B. Kellogg, V. Talla, S. Gollakota, and J. R. Smith, "Passive Wi-Fi: bringing low power to Wi-Fi Ttransmissions," in *USENIX Symposium on Networked Systems Design and Implementation (NSDI)*, Santa Clara, USA, 2016, pp. 1-14.
- [19] S. Roy, V. Jandhyala, J. R. Smith, D. Wetherall, and B. P. Otis, "RFID: from supply chains to sensor nets," *IEEE Proceedings*, vol. 98, no. 9, pp. 1583-1591, Sept. 2010.
- [20] S. Gollakota, M. S. Reynolds, J. R. Smith, and D. Wetherall, "The emergence of RF-powered computing," *IEEE Computer*, vol. 47, pp. 32-39, Jan. 2014.
- [21] M. Dong and L. Tong, "Optimal design and placement of pilot symbols for channel estimation," *IEEE Trans. Signal Process.*, vol. 50, no. 12, pp. 3055-3069, Dec. 2002.
- [22] C. Xing, S. Ma, and Y. Zhou, "Matrix-monotonic optimization for MIMO systems," *IEEE Trans. Signal Process.*, Vol. 63, no. 2, pp.334-348, Jan. 2015.
- [23] Z. Ma, T. Zeng, G. Wang, and F. Gao, "Signal detection for ambient backscatter system with multiple antennas," in *Proc. IEEE 14th Canadian Workshop on Information Theory (CWIT)*, St. John's, NL, Canada, 2015, pp. 1-4.
- [24] G. Wang, F. Gao, Z. Dou, and C. Tellambura, "Uplink detection and BER analysis for ambient backscatter communication systems," in *Proc. IEEE Globecom*, San Diego, CA, USA, 2015, pp. 1-5.
- [25] F. Fuschini, C. Piersanti, F. Paolazzi, and G. Falciasecca, "Analytical approach to the backscattering from UHF RFID transponder," *IEEE Antennas Propag. Lett.*, vol. 7, pp. 33-35, 2008.
- [26] A. Papoulis and S. U. Pillai, *Probability, Random Variables and Stochastic Processes*, 4th ed., New York: McGraw-Hill, 2002, ch. 7, pp. 278-279.
- [27] D. Tse and P. Viswanath, *Fundamentals of Wireless Communication*. Cambridge University Press, 2005.
- [28] M. Chiani, D. Dardari, and M. K. Simon, "New exponential bounds and approximations for the computation of error probability in fading channels," *IEEE Trans. Wireless Commun.*, vol. 2, pp. 840-845, July 2003.
- [29] J. T. Lin, "Approximating the normal tail probability and its inverse for use on a pocket calculator," *Appl. Statist.*, 38: no. 1, pp. 69-70, 1989.
- [30] T. Kailath and H. V. Poor, "Detection of Sthchastic processes," *IEEE Trans. Inf. Theory*, vol. 44, no. 6, pp. 2230-2259, Oct. 1998.
- [31] Y. Zou, X. Wang, W. Shen and L. Hanzo, "Security versus reliability analysis of opportunistic relaying," *IEEE Trans. Veh. Tech.*, vol. 63, no. 6, pp. 2653-2661, July 2014.
- [32] Y. Zou, J. Zhu, X. Wang and V. C. M. Leung, "Improving physical-layer security in wireless communications using diversity techniques," *IEEE Network*, vol. 29, no. 1, pp. 42-48, Jan.-Feb. 2015.
- [33] X. Cheng, Q. Yao, M. Wen, C. X. Wang, L. Y. Song, and B. L. Jiao, "Wideband channel modeling and intercarrier interference cancellation for vehicle-to-vehicle communication systems," *IEEE J. Sel. Areas Commun.*, vol. 31, no. 9, pp. 434-448, Sep. 2013.
- [34] X. Cheng, Y. L. Guan, and S. Li, "Optimal BER-balanced combining for weighted energy detection of UWB OOK signals," *IEEE Commun. Letter*, vol. 17, no. 2, pp. 353-356, Feb. 2013.



Gongpu Wang received the B.Eng. degree in communication engineering from Anhui University, Hefei, China, in 2001 and the M.Sc. degree from Beijing University of Posts and Telecommunications (BUPT), China, in 2004. From 2004 to 2007, he was an assistant professor in the School of Network Education, BUPT. He received the Ph.D. degree from the University of Alberta, Edmonton, Canada, in 2011. After graduation, he joined the School of Computer and Information Technology, Beijing Jiaotong University (BJTU), China, where he is currently an associate professor. His research interests include Internet of Things (IoT), wireless communication theory and signal processing technologies.



Feifei Gao (M'09, SM'14) received the B.Eng. degree from Xi'an Jiaotong University, Xi'an, China in 2002, the M.Sc. degree from McMaster University, Hamilton, ON, Canada in 2004, and the Ph.D. degree from National University of Singapore, Singapore in 2007. He was a Research Fellow with the Institute for Infocomm Research (I2R), A*STAR, Singapore in 2008 and an Assistant Professor with the School of Engineering and Science, Jacobs University, Bremen, Germany from 2009 to 2010. In 2011, he joined the Department of Automation, Tsinghua University, Beijing, China, where he is currently an Associate Professor.

Prof. Gao's research areas include communication theory, signal processing for communications, array signal processing, and convex optimizations, with particular interests in MIMO techniques, multi-carrier communications, cooperative communication, and cognitive radio networks. He has authored/coauthored more than 80 refereed IEEE journal papers and more than 120 IEEE conference proceeding papers, which have been cited more than 3500 times from Google Scholar.

Prof. Gao has served as an Editor of IEEE Transactions on Wireless Communications, IEEE Communications Letters, IEEE Signal Processing Letters, IEEE Wireless Communications Letters, International Journal on Antennas and Propagations, and China Communications. He has also served as the symposium co-chair for 2015 IEEE Conference on Communications (ICC), 2014 IEEE Global Communications Conference (GLOBECOM), 2014 IEEE Vehicular Technology Conference Fall (VTC), as well as Technical Committee Members for many other IEEE conferences.



Rongfei Fan received the B.E. degree in electrical engineering from Harbin Institute of Technology, Harbin, China, in 2007, and the Ph. D degree in electrical engineering from the University of Alberta, Edmonton, Alberta, Canada, in 2012. Since 2013, he has been a faculty member at the Beijing Institute of Technology, Beijing, China, where he is currently an Assistant Professor in the School of Information and Electronics. His research interest includes cognitive radio, cross-layer design, radio resource management for wireless communications

and energy harvesting.



Chintha Tellambura (F'11) received the B.Sc. degree (with first-class honors) from the University of Moratuwa, Moratuwa, Sri Lanka, in 1986, the M.Sc. degree in electronics from the University of London, London, U.K., in 1988, and the Ph.D. degree in electrical engineering from the University of Victoria, Victoria, BC, Canada, in 1993.

He was a Postdoctoral Research Fellow with the University of Victoria (1993-1994) and the University of Bradford (1995-1996). He was with Monash University, Melbourne, Australia, from 1997 to 2002.

Presently, he is a Professor with the Department of Electrical and Computer Engineering, University of Alberta. His research current interests include multiple antenna and multicarrier communication systems, cognitive radio and relay networks.